J. Fluid Mech. (2003), *vol.* 485, *pp.* 1–32.
DOI: 10.1017/S0022112003003975 Printed in the United Kingdom

Skin-friction measurements in high-enthalpy hypersonic boundary layers

By C. P. GOYNE†, R. J. STALKER AND A. PAULL

Department of Mechanical Engineering, University of Queensland, Queensland 4072, Australia

(Received 12 March 2002 and in revised form 16 December 2002)

Skin-friction measurements are reported for high-enthalpy and high-Mach-number laminar, transitional and turbulent boundary layers. The measurements were performed in a free-piston shock tunnel with air-flow Mach number, stagnation enthalpy and Reynolds numbers in the ranges of 4.4–6.7, 3–13 MJ kg^{-1} and 0.16×10^6–21×10^6, respectively. Wall temperatures were near 300 K and this resulted in ratios of wall enthalpy to flow-stagnation enthalpy in the range of 0.1–0.02. The experiments were performed using rectangular ducts. The measurements were accomplished using a new skin-friction gauge that was developed for impulse facility testing. The gauge was an acceleration compensated piezoelectric transducer and had a lowest natural frequency near 40 kHz. Turbulent skin-friction levels were measured to within a typical uncertainty of $\pm7\%$. The systematic uncertainty in measured skin-friction coefficient was high for the tested laminar conditions; however, to within experimental uncertainty, the skin-friction and heat-transfer measurements were in agreement with the laminar theory of van Driest (1952). For predicting turbulent skin-friction coefficient, it was established that, for the range of Mach numbers and Reynolds numbers of the experiments, with cold walls and boundary layers approaching the turbulent equilibrium state, the Spalding & Chi (1964) method was the most suitable of the theories tested. It was also established that if the heat transfer rate to the wall is to be predicted, then the Spalding & Chi (1964) method should be used in conjunction with a Reynolds analogy factor near unity. If more accurate results are required, then an experimentally observed relationship between the Reynolds analogy factor and the skin-friction coefficient may be applied.

1. Introduction

Skin friction plays a fundamental role in boundary-layer studies. For example, it measures the transfer of momentum from the flow to the surface and is therefore an important input to integral calculations involving the boundary layer. It is also a measure of the velocity gradient at the surface, and thus influences the velocity profile of the boundary layer. Also, for turbulent boundary layers, it provides the basis for a widely accepted correlation of velocity profiles.

In engineering, skin friction is an important source of drag, particularly at hypersonic speeds. This can be illustrated by considering a flat plate at incidence at a Mach number of 16. With a turbulent boundary layer, a mean skin-friction coefficient on the windward surface might be 1.7×10^{-3}. Then, it is readily found

† Present address: Aerospace Research Laboratory, Department of Mechanical and Aerospace Engineering, University of Virginia, Charlottesville, VA 22904, USA.

that the skin-friction drag is equal to the inviscid drag at an angle of incidence of 7°. At lower angles, skin friction exceeds the inviscid drag. Thus, skin friction is likely to have a crucial effect on the performance of slender hypersonic vehicles.

In contrast to its scientific and engineering importance, skin friction has not been extensively measured in flows that simulate hypersonic flight, i.e. flows with Mach numbers in excess of 4–5 and stagnation enthalpies above $1\,\mathrm{MJ\,kg^{-1}}$. For laminar boundary layers in high-enthalpy hypersonic flow, skin friction has not been the subject of intensive experimental work, largely because laminar theory has a well-established physical basis, and can be verified through heat-transfer measurements, such as those of East, Stalker & Baird (1980). The skin-friction levels can be related to heat-transfer levels through Reynolds analogy, and this can be performed with a high degree of confidence. There are also very few measurements of skin friction in transitional high-enthalpy hypersonic boundary layers. Holden (1972) used a shock tunnel to obtain limited skin-friction measurements in the transition region. Much work has been done on transition in high-enthalpy hypersonic flow using measurements of surface heat transfer (e.g. He & Morgan 1994; Mee & Goyne 1996; Adam & Hornung 1997) but, in the absence of a physical understanding that leads to quantitative relations between heat transfer and skin friction, this work does not lead to reliable predictions of skin friction.

The measurement of the skin friction in high-enthalpy hypersonic turbulent boundary layers has received considerably more attention. This is indicated by the data sets used in reviews of compressible turbulent skin friction by Hopkins & Inouye (1971), Cary & Bertram (1974) and Bradshaw (1977). For laminar boundary layers, the Howarth–Dorodnitsyn compressibility transformation allows compressible skin friction to be related to values for a corresponding incompressible boundary layer. The fact that values for incompressible turbulent skin friction are well known suggests that suitable transformations might be found for compressible turbulent boundary layers which will relate them to incompressible boundary layers, and the three reviews mentioned above evaluate the success of attempts to develop such transformations. They conclude that none of the transformations developed can be used with confidence outside the range over which they have been tested experimentally. The same would apply to the Reynolds analogy factor.

It can be expected that hypersonic-flight Mach numbers will imply high stagnation enthalpy flow with relatively low surface enthalpies. Previous investigations have been limited to stagnation enthalpies near $1\,\mathrm{MJ\,kg^{-1}}$ or, for the limited shock-tunnel data available, near $2\,\mathrm{MJ\,kg^{-1}}$. There is therefore a lack of experimental hypersonic skin-friction data in the regime of high stagnation enthalpy turbulent boundary-layer flow, with low ratios of surface to stagnation enthalpies, i.e. $h_w/h_0 \lesssim 0.2$ (e.g. see Hopkins & Inouye 1971; Coleman, Osborne & Stollery 1973; Anderson, Kumar & Erdos 1990). Thus, the objectives of this investigation are; through use of a shock tunnel, first, to measure skin friction in constant-pressure boundary layers, over a Reynolds-number range allowing laminar, transitional and turbulent boundary layers, at stagnation enthalpies up to $9\,\mathrm{MJ\,kg^{-1}}$ (and higher, where possible) and, secondly, to evaluate the accuracy of popular analytical methods for predicting turbulent boundary-layer skin friction at stagnation enthalpies up to $9\,\mathrm{MJ\,kg^{-1}}$.

Given the uncertainty of skin-friction prediction in high-enthalpy turbulent boundary layers, the paper begins with a discussion of popular analytical theory that is available for such flows. Previous experimental comparisons by other investigators are then summarized. The paper then presents a description of the characteristics of the shock tunnel, together with the model and instrumentation used for the experiments.

A brief survey of the results for both skin friction and heat transfer is then given. In light of existing analytical skin-friction theory, the results for the laminar and turbulent boundary layers are considered. This is then followed by a discussion of the measured turbulent Reynolds analogy factor before leading on to the conclusions.

2. Turbulent boundary layers

2.1. *Analytical theories*

As noted in § 1, considerable effort has gone into the development of transformations which will relate the properties of compressible turbulent boundary layers to a corresponding incompressible case. This approach can be justified by Morkovin's hypothesis. Spina, Smits & Robinson (1994) explain Morkovin's hypothesis in these terms: the dynamics of a compressible turbulent boundary layer will follow the incompressible pattern closely if the Mach-number fluctuations remain small (e.g. $M' \leqslant 0.3$). For zero-pressure-gradient adiabatic boundary layers, Morkovin's hypothesis is generally valid up to a free-stream Mach number (M_e) range of 4–5 (Bradshaw 1977; Spina *et al.* 1994). Beyond Mach 5, the near-wall region of the boundary layer is likely to exhibit significant departure from the known incompressible structure (Spina *et al.* 1994).

One of the most popular analytical compressible skin-friction solutions for turbulent boundary layers, known as van Driest II (1956), was developed using a mixing-length approximation. Van Driest extended his 1951 work (van Driest 1951) and adapted the von Kármán mixing-length hypothesis for incompressible flow. Such a hypothesis relates the eddy viscosity to some characteristic length scale. According to Morkovin's hypothesis, the turbulence structure will be the same in the compressible case for about $M_e \leqslant 5$, and hence a solution will be valid if appropriate compressibility scaling is incorporated. Van Driest assumed a calorically perfect gas with a Prandtl number of unity and the turbulent Crocco relation was used to determine density and velocity profiles in the boundary layer. The skin friction was then obtained using the boundary-layer momentum thickness and the Kármán integral relation (see White 1991). Morkovin's hypothesis, used in similar ways, has formed the basic justification for all the popular analytical methods for predicting compressible turbulent skin friction and wall heat flux. Bradshaw (1977) provides a thorough review of the methodology.

Spalding & Chi (1964) used a similar transformation, with empirical input, and introduced a generic form of the relations for compressible turbulent skin friction. Hopkins & Inouye (1971) later showed that all the methods based on Reynolds number, Mach number and T_w/T_e, including van Driest II (1956) and reference temperature concepts such as Eckert (1955), could be reduced to the Spalding & Chi canonical form. This allowed compressible flow experimental data, obtained over a range of test conditions, to be compared directly to a single incompressible skin-friction relation. The compressibility transformation can be represented by

$$C_{f,i} = F_c C_f, \tag{1}$$

$$Re_{x,i} = F_{Re_x} Re_x. \tag{2}$$

The skin-friction coefficient is given by

$$C_f = 2\tau / \rho_e u_e^2,$$

where τ is the surface shear and ρ_e and u_e are the mainstream density and velocity,

respectively. The Reynolds number is given by

$$Re_x = \rho_e u_e x/\mu_e,$$

where x is the distance from the leading edge, and μ_e is the mainstream viscosity. The subscript i denotes an incompressible value. For a constant ratio of specific heats, the factors F_{Re_x} and F_c are functions of Mach number, free-stream static temperature, wall temperature and recovery factor only. The calculation procedure for a given Reynolds number, Re_x, then is, (i) the incompressible skin-friction coefficient is calculated using $(Re_x \times F_{Re_x})$ as an input to an accepted incompressible relation; and (ii) this coefficient is divided by F_c to obtain the compressible skin-friction coefficient. In essence, the incompressible skin-friction relation is simply scaled for compressibility. If required, the heat flux to the wall is then computed using a turbulent Reynolds analogy factor $(2C_h/C_f)$ and a definition of the Stanton number of

$$C_h = \frac{\dot{q}}{\rho_e u_e (h_{aw} - h_w)},$$

where $\dot{q}$ is the heat flux to the wall and h_w and h_{aw} is the wall and adiabatic wall enthalpy, respectively. Here, the adiabatic wall enthalpy is given by $h_{aw} = h_e + \frac{1}{2} r u_e^2$, h_e is the enthalpy of the mainstream, and r is the recovery factor.

The transformation factors F_c and F_{Re_x} for four popular turbulent skin-friction theories are given below. An adiabatic wall temperature is used in the correlations and was calculated here using the adiabatic wall enthalpy and assuming a calorically perfect gas, i.e.

$$T_{aw} = \frac{h_{aw}}{c_p},$$

where c_p is the constant-pressure specific heat. The calorically perfect gas concept of an adiabatic wall temperature becomes less valid at conditions of high stagnation enthalpy. However, it can be shown using the Crocco relation (e.g. White 1991) that the assumption of a calorically perfect gas is valid, within the boundary layer, to free-stream stagnation temperatures in the range of 3200–4000 K. Hence, for the flow conditions of interest for the present study, the effect of using an adiabatic wall temperature is expected to be small.

Two studies have investigated means of removing the perfect gas assumptions from the conventional compressible turbulent correlations. Using the Crocco relation, Wallace (1967) modified the correlation of Spalding & Chi (1964), and more recently, Hazelton & Bowersox (1998) examined the effect of the calorically perfect gas assumption on skin-friction levels predicted by van Driest II (1956). When compared to a high-enthalpy modified form, the perfect gas theory increasingly underestimated C_f as the free-stream Mach number and, hence, flow stagnation enthalpy was increased. However, up to a stagnation enthalpy of $7\,\mathrm{MJ\,kg^{-1}}$, the maximum difference between the two forms of the theory was 5%. Less than 9% of the turbulent data of the present study were collected above $7\,\mathrm{MJ\,kg^{-1}}$, hence again, the effects of the calorically perfect gas assumption on predicted turbulent skin-friction levels are expected to be small. Therefore, for consistency with the analyses of Cary & Bertram (1974), Hopkins & Inouye (1971), Holden (1972) and Stollery (1976), the use of an adiabatic wall temperature is retained.

For the present study, a turbulent recovery factor of $r \approx Pr^{1/3} \approx 0.89$ was adopted. This is in accord with the recommendations of White (1991) and Cary & Bertram (1974).

The compressible turbulent boundary-layer transformation factors for each of the chosen correlations are as follows. For the first three correlations, the form of the equations are the same as those used by Cary & Bertram (1974).

2.1.1. *Van Driest II* (1956)

$$F_c = \frac{T_{aw}/T_e - 1}{(\sin^{-1}\kappa + \sin^{-1}\nu)^2}, \tag{3}$$

$$F_{Re_x} = \frac{\mu_e}{\mu_w}\frac{1}{F_c}, \tag{4}$$

where

$$\kappa = \frac{T_{aw}/T_e + T_w/T_e - 2}{\sqrt{(T_{aw}/T_e + T_w/T_e)^2 - 4T_w/T_e}}, \tag{5}$$

$$\nu = \frac{T_{aw}/T_e - T_w/T_e}{\sqrt{(T_{aw}/T_e + T_w/T_e)^2 - 4T_w/T_e}}, \tag{6}$$

the subscripts w and e indicating conditions at the wall and in the mainstream, respectively.

2.1.2. *Spalding & Chi* (1964)

$$F_c = \frac{T_{aw}/T_e - 1}{(\sin^{-1}\kappa + \sin^{-1}\nu)^2}, \tag{7}$$

$$F_{Re_x} = (T_{aw}/T_e)^{0.772}(T_w/T_e)^{-1.474}\ 1/F_c, \tag{8}$$

where κ and ν are given by equations (5) and (6).

2.1.3. *Eckert* (1955)

$$F_c = T^*/T_e, \tag{9}$$

$$F_{Re_x} = \frac{\mu_e T_e}{\mu^* T^*}, \tag{10}$$

where the reference temperature is given by

$$T^* = 0.5T_w + 0.22T_{aw} + 0.28T_e. \tag{11}$$

2.1.4. *Stollery* (1976)

For the present study, the transformation factors F_c and F_{Re_x} are the same as Eckert's (equations (9) and (10), respectively). To determine the coefficient of skin friction in an isentropic pressure gradient, Stollery used the concept of local flat-plate equivalence, an incompressible one-fifth power law for skin friction (e.g. Schlichting 1979) and Eckert's reference temperature (equation (11)). The relation obtained for the free-stream properties based skin friction coefficient is

$$\tfrac{1}{2}C_{f,\infty} = 0.0296\left(\frac{T_e}{T^*}\right)^{3/5}\left(\frac{M_e}{M_\infty}\right)^{9/5}\Pi^{(11\gamma-3)/10\gamma}\left(\frac{C}{Re_x}\right)^{1/5}, \tag{12}$$

where C is defined through

$$\frac{\mu^*}{\mu_e} = C\frac{T^*}{T_e},$$

and where γ is the ratio of the specific heats, M is the Mach number and $\Pi(=P_e(x)/P_\infty)$, is the ratio of local pressure to the far-field free-stream static pressure. In Stollery's study, and in the calculations here, the viscosity constant, C, was approximated as unity for simplicity (the Sutherland viscosity formula was used for all other calculations here, however).

In order to assess first the applicability of this theory for the present study, it is applied to a constant pressure flow. In this case $\Pi = 1$, and, hence, the transformation factors, F_c and F_{Re_x}, become the same as that of Eckert's. However, the incompressible skin-friction coefficient is now calculated using the one-fifth power law in Schlichting (1979), given by

$$\tfrac{1}{2}C_{f,i} = 0.0296(Re_{x,i})^{-1/5} \tag{13}$$

2.2. *Previous experimental comparisons*

At this point, it is appropriate to note the outcome of previous comparisons of experimental data with the theories under consideration. Two of the most comprehensive reviews of turbulent skin-friction data of high-enthalpy flows were performed by Hopkins & Inouye (1971) and Cary & Bertram (1974).

Hopkins & Inouye (1971) compared direct skin-friction measurements on non-adiabatic flat plates with the theories of van Driest II (1956), Spalding & Chi (1964), and others. Free-stream conditions varied from Mach 2.8 to Mach 7.4 with a range of wall to stagnation enthalpy ratio of approximately 0.14–1.0. The skin-friction data used in the comparison were obtained by Hopkins *et al.* (1969), Wallace & McLaughlin (1966), Neal (1966), Young (1965) and Sommer & Short (1955). Boundary-layer trips were used in some of the experiments. Hopkins & Inouye found that for $T_w/T_{aw} > 0.3$, the theory of van Driest II predicted the skin friction to within about 10%, but failed at lower temperature ratios. $(C_{f,exp}/C_{f,the} - 1)$ generally decreased as T_w/T_{aw} was decreased below 0.3, becoming as low as approximately -0.2 for van Driest II at T_w/T_{aw} of 0.14 (i.e. theory overpredicted experiment by 20%). Here, $C_{f,exp}$ and $C_{f,the}$ are the experimentally measured and theoretically predicted skin-friction coefficients, respectively. At a wall temperature ratio of 0.14, Spalding & Chi (1964) were the most in agreement with experiment. After further comparisons, using heat-transfer data and adiabatic flat-plate and non-adiabatic wind-tunnel wall skin-friction data, Hopkins & Inouye (1971) recommended the theory of van Driest II.

Cary & Bertram (1974) used turbulent skin-friction and heat-transfer data for flat plates and cones. The skin-friction data represented a free-stream Mach-number range of 6–13, a ratio of wall to stagnation enthalpy of 0.14–0.46 and an approximate unit Reynolds-number range of 5×10^6–$2 \times 10^8\,\mathrm{m}^{-1}$. The skin-friction experiments were performed by Hopkins *et al.* (1969, 1972), Heronimus (1966), Wallace (1967) and Holden (1972). Cary & Bertram (1974) evaluated the turbulent theories of van Driest II (1956), Spalding & Chi (1964) and Eckert (1955) (amongst others). They concluded that the Spalding & Chi method gave the best prediction for free-stream Mach numbers less than 10. For higher Mach numbers, they commented that differences between theory and experiment may have been due to the boundary layer not reaching the turbulent equilibrium state, i.e. the flow was more equivalent to low-Reynolds-number turbulent flows.

A later review by Bradshaw (1977) questioned Cary & Bertram's choice of Spalding & Chi (1964). Heat-transfer data were included in Cary & Bertram's study because of the lack of available skin-friction data. As all the theories predicted skin friction, this required the assumption of a Reynolds analogy factor which is ill-defined at high-enthalpy conditions. Bradshaw (1977) also commented that Hopkins & Inouye's choice of van Driest II (1956) was justifiable, however, like all of the turbulent boundary-layer theories, van Driest II (1956) failed to predict the fall in skin-friction coefficient that apparently occurred on very cold walls ($T_w/T_{aw} \leqslant 0.1$–0.2).

Of particular interest to the present study are the skin-friction measurements obtained by Holden (1972). These measurements, which were performed in shock tunnels, represent the most recent high stagnation enthalpy skin-friction data that are available for zero-incidence flat plates. The skin-friction gauges that were used employed piezoelectric elements acting in the bending mode, and are described by Holden (1972). The free-stream Mach number ranged from 7 to 13, the ratio of wall to stagnation enthalpy ranged from 0.14 to 0.3 and Reynolds numbers and unit Reynolds numbers varied between 6×10^6 and 180×10^6 and $17 \times 10^6\,\mathrm{m}^{-1}$ and $190 \times 10^6\,\mathrm{m}^{-1}$, respectively. The theories of van Driest II (1956), Spalding & Chi (1964) and Eckert (1955) were compared. Holden concluded that the theory of Spalding & Chi was in best agreement with experiment in the Mach 7–10 range. Van Driest II and Eckert tended to overpredict in this range. However, in the Mach 10–13 range, van Driest II and Eckert predicted the skin-friction levels best and Spalding & Chi underpredicted. The same general results were obtained using Reynolds numbers based on momentum thickness or distance from a turbulent virtual origin. Holden was unable to determine whether the disagreement between Spalding & Chi and the high-Mach-number data resulted from a low-Reynolds-number effect (remnants from the transition process), or an inadequacy of the theory. It is worth noting here that Holden's high-Mach-number data generally corresponded to lower-flow unit Reynolds numbers.

Thus, in summary, the previous experimental comparisons yielded differences in the theory finally recommended. Apart from the theory of Stollery (1976), which has not been compared to high-enthalpy data, there was a tendency for all the theories to predict skin friction in excess of the measured value on very cold walls. Furthermore, the theories increasingly overpredicted as the ratio of wall temperature to adiabatic wall temperature (T_w/T_{aw}) was reduced. The present study not only allows further comparison of the theories with experiment but, because the range of tunnel stagnation enthalpies covered allowed a value of T_w/T_{aw} to be reached that was a factor of 5 less than in previous experiments, it provides a particular opportunity of observing the trend at low T_w/T_{aw}.

3. Experiment

3.1. *Shock tunnel operation*

The experiments were performed in the free-piston shock tunnel T4 at the University of Queensland. The shock tunnel consists of an air reservoir, $0.68\,\mathrm{m}^3$ in volume, which is used in driving a free piston along a 27 m long, 228 mm diameter compression tube. This process raises the temperature and pressure of the shock-tube driver gas (located in the compression tube) immediately prior to rupture of the shock-tube main diaphragm. The shock tube was 10 m long and 76 mm in diameter, and was located at the downstream end of the compression tube. It supplied heated and compressed air test gas to a 0.8 m long contoured hypersonic nozzle. The nozzle expanded from

Condition	T (K)	P (kPa)	ρ (kg m^{-3})	u (m s^{-1})	M	$Re_u \times 10^6$ (m^{-1})	Y_O	Y_{NO}	h_0 (MJ kg^{-1})
A	486	0.87	0.0063	2800	6.4	0.669	n/a	n/a	4.4
B	772	1.03	0.0045	3460	6.2	0.434	0.0429	0.0624	7.8
C	1010	2.70	0.0090	3740	5.9	0.789	0.0405	0.0666	9.1
D	331	4.14	0.0436	2430	6.7	5.33	n/a	n/a	3.3
E	541	4.38	0.0282	2900	6.3	2.91	n/a	n/a	4.8
F	630	5.09	0.0280	3050	6.1	2.74	n/a	n/a	5.3
G	1010	5.14	0.0174	3670	5.8	1.52	0.0187	0.0683	8.4
H	326	5.82	0.0623	2400	6.6	7.60	n/a	n/a	3.2
I	784	8.03	0.0356	3330	6.0	3.31	0.0034	0.0671	6.7
J	1160	9.41	0.0278	3800	5.7	2.33	0.0161	0.0673	9.1
K	351	9.20	0.0912	2470	6.6	10.9	n/a	n/a	3.4
L	740	12.5	0.0589	3250	6.0	5.53	0.0014	0.0644	6.3
M	1270	15.7	0.0430	3880	5.6	3.50	0.0122	0.0666	9.4
N	1790	17.2	0.0320	4430	5.3	2.44	0.0462	0.0604	13.1
Q	336	13.4	0.1395	2400	6.5	16.6	n/a	n/a	3.2
R	810	17.9	0.0770	3330	5.9	7.01	0.0013	0.0637	6.6

TABLE 1. Test conditions.

a throat diameter of 25 mm to a diameter of 262 mm at the test section. The nozzle supply pressure was monitored by a PCB^{TM} type piezoelectric pressure transducer located near the downstream end of the shock tube. Pitot surveys of the nozzle flow at a typical test condition are presented in Paull, Stalker & Mee (1995). They exhibit a test core of essentially uniform flow approximately 200 mm in diameter.

Nozzle supply conditions were determined by obtaining the post-shock reflection pressure and stagnation enthalpy from measurements of the shock speed and shock-tube filling pressure and, when required, assuming a subsequent isentropic expansion to the measured nozzle supply pressure. The nozzle supply conditions were varied through a range of stagnation enthalpies and pressures by varying the driver gas compression ratio in the compression tube, the pressure levels throughout the shock tunnel and the mixture ratio in the argon–helium driver gas mixture. In this way, a range of values for the test-section stagnation enthalpy and unit Reynolds number could be obtained, while producing nearly steady nozzle supply conditions during the test time.

The test section conditions used in the experiments are summarized in table 1, where T, P, ρ, u, M, Re_u, Y_O, Y_{NO} and h_0 are, respectively, the temperature, pressure, density, velocity, Mach number, unit Reynolds number, oxygen atom mass fraction and nitric oxide mass fraction and stagnation enthalpy. These were calculated using a one-dimensional non-equilibrium nozzle flow code adapted from Lordi, Mates & Moselle (1966), whereby the flow was expanded until it reached the mean measured Pitot pressure in the test duct. Measurements with a mass spectrometer by Skinner & Stalker (1996) have indicated that oxygen atom mass fractions are lower than the values quoted, and the nitric oxide mass fractions are somewhat higher, but in the absence of a theoretical model which reconciles these differences, the values shown are given as an indication of the presence of non-equilibrium species. For stagnation enthalpies of 5.3 MJ kg^{-1} and lower, the instability of calculations performed using the code made it necessary to employ an equilibrium calculation.

The test flow Pitot pressure was monitored with a probe mounted on the side of the model. The probe was mounted such that the point of measurement was

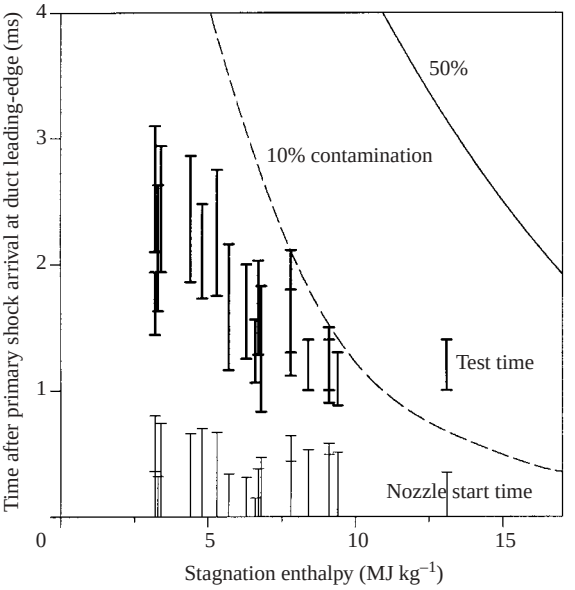

FIGURE 1. Test period and nozzle starting times compared with driver gas contamination times.

at approximately the same axial location as the inlet of the model. In a separate series of tests, at 3.4 MJ kg^{-1} and 9.4 MJ kg^{-1}, the Pitot pressure was measured at three axial positions in the duct, and this allowed determination of the mean ratio of Pitot pressure in the duct to that measured by the monitoring probe as: $(P_{Pitot})_{duct}/(P_{Pitot})_{monitor} = 0.86 \pm 0.09$. The Pitot pressure decayed by approximately 15% along the duct length.

Conservative estimates by Mee (1993) yield the uncertainty in the Pitot pressure as $\pm 8\%$, and the uncertainty of the static temperature, pressure and density as $\pm 12\%$, $\pm 15\%$ and $\pm 13\%$, respectively, while the uncertainty in each of the velocity and the Mach number is $\pm 5\%$. The repeatability of each of these quantities over a typical series of tests at the same condition is, in the same order, $\pm 2\%$, $\pm 2\%$, $\pm 3\%$, $\pm 2.5\%$, $\pm 0.6\%$ and $\pm 0.7\%$. In shock-tunnel testing, it is important to know when the test flow becomes contaminated by driver gas. Experiments by Skinner (1994) and Boyce, Takahashi & Stalker (1996), using a mass spectrometer, and by Paull (1996), using a simple gas dynamic driver gas detector, have allowed construction of the curves in figure 1. These curves indicate the variation with time and stagnation enthalpy of the approximate level of driver gas contamination. The test period is also shown for all test conditions, and it can be seen that this falls within the period when the flow is essentially free of contamination for all but the highest enthalpy condition, *N*. At this condition, the driver gas argon:helium mixture ratio was 13:87.

3.2. *The model*

A diagram of the model used in the experiment is given in figure 2. The limited size of the shock tunnel implied that, in order to produce the range of Reynolds numbers required for the experiments, whilst retaining a nominally uniform mainstream flow, it was necessary to employ a duct. The duct was of rectangular cross-section and one wall was instrumented for measurement of heat transfer, pressure and skin friction, as shown in the upper part of the figure. Because of the limited number of available

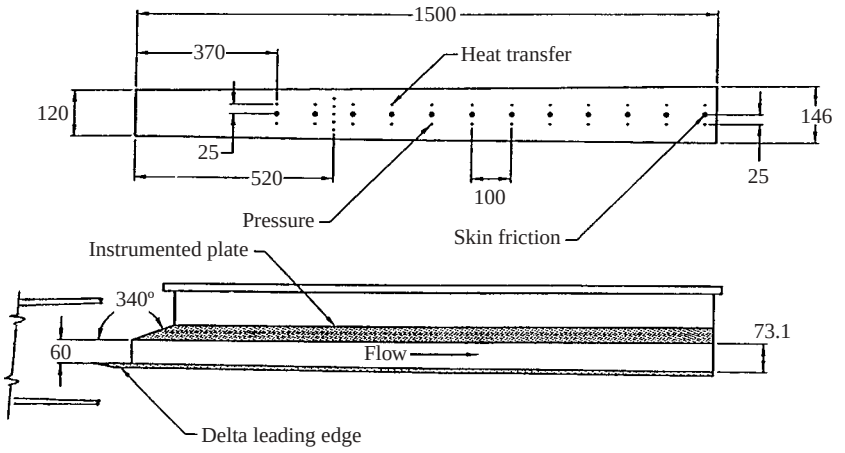

FIGURE 2. The test model (dimensions in mm).

skin-friction gauges, not all skin-friction tappings were used at one time. Unused tappings were sealed using gauge blanks. The lower part of figure 2 shows the duct in elevation, and its approximate position in relation to the shock-tunnel nozzle exit. Manufacturing tolerances and surface finish combined to ensure that the walls within the duct were hydraulically smooth (White 1991). Given the duct wall temperature and levels of test gas total temperature and dissociation, the plate surface was expected to be non-catalytic. The duct wall temperature remained at 300 K throughout the tests.

In order to simulate a flat-plate constant-pressure boundary-layer flow as closely as possible, the non-instrumented duct walls were mounted with a small divergence of 0.5°. To compensate for leading-edge viscous interaction, the wall opposite the instrumented surface was provided with a delta leading edge, which had the effect of 'smearing' the leading-edge interaction waves. As shown in figure 2, five pressure transducers were located on a transverse line at the 520 mm station, and these indicated that no significant transverse pressure gradients resulted from the leading edge. Typical static pressure distributions along the duct are displayed in figure 3, with the test condition indicated for each distribution. They show that, for the purposes of the experiments, the static pressure may be regarded as essentially constant along the duct (the standard deviation in pressure level along the duct was typically 7.5%).

The choice of the model inlet dimensions was governed by the requirement of minimizing corner and secondary-flow effects on the instrumented plate boundary layer, while simultaneously ensuring that the inlet was not larger than the uniform core flow region of the nozzle.

Corner effects were studied by Stainback & Weinstein (1967). This study, which included unbounded perpendicular corners aligned with the flow, indicated turbulent boundary layers are significantly less sensitive to corner interaction than laminar boundary layers. Measurements of heat transfer at Mach 8 and $Re_x = 1.5 \times 10^6$ indicated that a laminar boundary layer was significantly affected ($\geqslant$15%) by the corner region up to 15 mm from the corner. Data from turbulent boundary layers at Mach 5 and $Re_x = 2 \times 10^7$ and 5×10^7 showed no significant corner influence as close as 3 mm to the corner.

Davis, Gessner & Kerlick (1986, 1987) studied bounded laminar and turbulent corner boundary layers numerically and experimentally in a duct. The model consisted

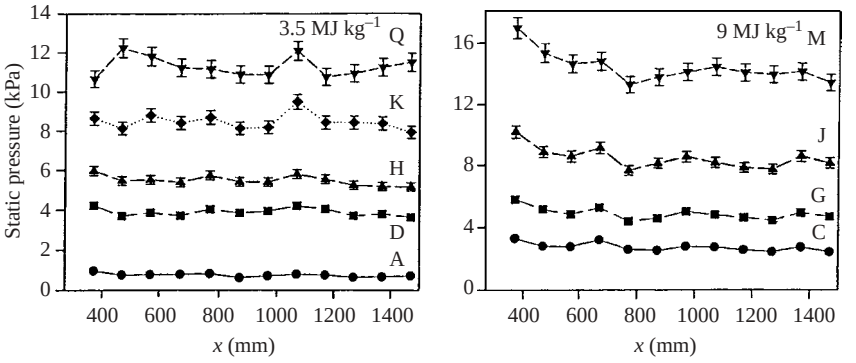

FIGURE 3. Typical axial static pressure distributions along instrumented surface.

of a $25 \times 25\,\text{mm}^2$ duct with an adverse pressure gradient flow. The studies showed that secondary flows adjacent to the corners of the duct were evident. However, the flows only significantly influenced ($\geqslant$15%) the instrumented plate skin friction to a distance of 5% of the duct width.

Although the models of the above studies are not geometrically the same as the present rectangular duct (which has an aspect ratio of 2), the available evidence indicates that the surface measurements of the present study, obtained at 35 mm from the corners of a 120 mm wide corner bounded plate, will not be significantly affected by corner and secondary flows, particularly for high-Reynolds-number flows. The choice of a $120 \times 60\,\text{mm}^2$ inlet therefore allowed minimal corner effects over the test surface, while permitting the inlet to remain within the Mach 6 nozzle core flow over a range of axial model locations. It is noted, however, that while fully laminar and fully turbulent boundary layers are expected to be largely unaffected by sidewall effects, a transitional boundary layer may be affected through transverse transition contamination (as in Korkegi 1956).

3.3. *Pressure and heat transfer measurement*

Pressure was measured using quartz piezoelectric pressure transducers made by PCB Piezotronics. The static pressure transducers were recess mounted with a pressure tapping, typically 2 mm in length and diameter, leading to the sensing surface. Typical measurement uncertainty was $\pm$4%.

Heat transfer rates were measured using platinum thin-film heat transfer gauges with a quartz substrate. The sensing platinum film was approximately 1 mm long, 0.2 mm wide and 0.75 μm in thickness. A 0.12 μm thick layer of silicon dioxide was vacuum deposited over the sensing face. Taking account of the effect of the presence of the platinum film on the heat transfer rate, the effect of temperature rise on the quartz thermal properties, the effect of calibration error in determination of the temperature coefficient of resistance of the gauges, and the effect of quartz substrate and model surface temperature differences, the uncertainty in the measured heat transfer rate was estimated at $\pm$8.5%.

3.4. *Skin friction measurement*

Skin friction was measured using a gauge design which was developed in the laboratory. The principle of operation of the gauge is shown in figure 4(*a*). The skin-friction force is applied through a floating element which is directly attached to a piezoceramic ring. The piezoceramic is mounted so that its direction of polarization

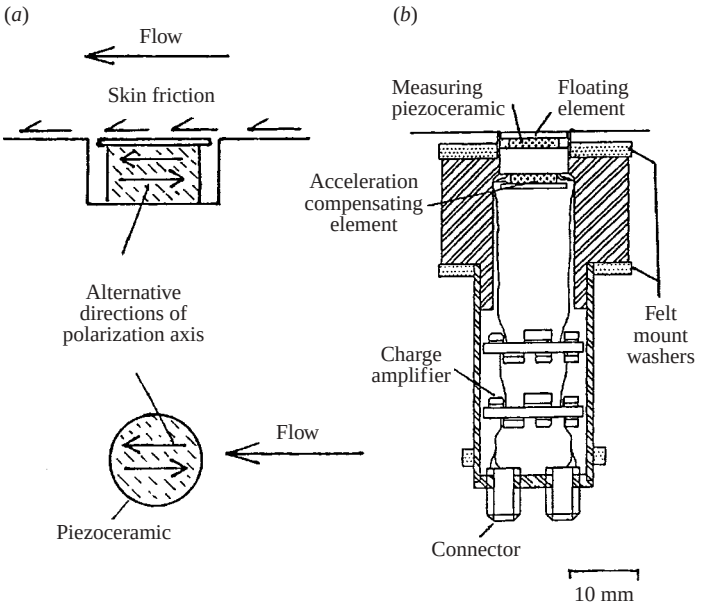

FIGURE 4. Skin-friction gauge. (*a*) Principle of operation. (*b*) Design layout.

is parallel to the direction of the skin-friction force to be measured. The design of the gauge is depicted in figure 4(*b*) and is fully described in Goyne, Stalker & Paull (2002). The gauge is essentially an acceleration compensated force transducer. It consists of a 10 mm diameter floating element that is exposed to the flow and an acceleration compensating element that is mounted internally. The acceleration compensating element and associated piezoceramic are of the same dimensions as the floating element and measuring piezoceramic, respectively. Both piezoceramics were mounted in a similar fashion, and as both were operated in shear mode, the ceramics were nominally equally sensitive to acceleration along the measurement axis. By monitoring the output of a charge amplifier connected to each piezoceramic, the gauge could be compensated for acceleration during service by subtraction of one signal from the other.

The skin-friction design integrated techniques to maximize rise time and this resulted in a transducer lowest natural frequency near 40 kHz. As described in Goyne *et al.* 2002, the gauge was calibrated for skin friction and acceleration in separate bench tests. Pressure calibrations were performed *in situ* during the shock-tunnel experiments reported here and elsewhere (Goyne *et al.* 1999). The characteristics of a typical skin-friction gauge are summarized in table 2.

Experimental uncertainty analyses were conducted for the calibration, compensation and measurement methods. Only small experimental errors were identified in the shear and acceleration calibration techniques and in the compensation and measurement methods. However, it was established that the pressure calibration technique introduced a large systematic relative error in the skin-friction measurements when skin-friction levels were low. Such was the case for the laminar boundary layers in the present study. For transitional and turbulent boundary layers, however, overall systematic uncertainty was much lower. Goyne *et al.* (2002) reports that for typical conditions of the present study, skin friction could be measured to within $\pm 47\%$, $\pm 16\%$ and $\pm 7\%$ for laminar, transitional and turbulent boundary layers, respectively.

Specifications	
Maximum calibrated range	0–4000 Pa
Resolution (with 30 μs time average)	1 Pa
Sensitivity (nominal at 296 K)	0.8×10^{-3} V Pa^{-1}
Linearity (zero-based best straight line)	1.5% FS
Cross-axis shear sensitivity	6%
Pressure sensitivity	4×10^{-3} V kPa^{-1}
Lowest resonant frequency	~40 kHz
Frequency range (approx.) (±5%)	20–10 000 Hz
(±10%)	15–12 000 Hz
Decay time constant	47 ms
Polarity (at 0°)	Positive
Maximum operating temperature	380 K
Temperature sensitivity	~0.5% K^{-1}
Maximum heat flux over 3 ms	7.5 MW m^{-2}
Maximum static pressure	~14 MPa
Sensing element diameter	10 mm
Element to housing gap (nominal)	0.16 mm
Piezoceramic material	PZT-5H
Sensing element material	Invar
Housing material	Brass
Total weight	98×10^{-3} kg
Excitation (constant current)	4 mA
Voltage to current regulator	12–24 V d.c.
Connector	B & K™ micro-dot × 2

TABLE 2. Specification summary for a typical skin-friction gauge.

3.5. *Data recording*

Data was recorded and stored on a 12 bit transient data storage device with a sampling time of 1 μs. The output from the skin friction gauges was directly recorded, while the output from the pressure transducers and the heat transfer gauges was recorded through 3× or 4× multiplexers, resulting in a sampling time of 3 or 4 μs for each channel. The signals recorded from the skin friction and pressure transducers were time averaged over a period of 30 μs before display. The signals from the thin-film heat transfer gauges were computer processed to determine the heat transfer rate and then time averaged over 30 μs.

4. Results

The experimental results of the present investigation are first presented in the form of time-resolved records of pressure, skin friction and heat transfer. Axial distributions of measured skin-friction coefficient and Stanton number during the test time are then examined. The laminar and turbulent skin friction and heat transfer levels are then discussed in depth in the section that follows.

4.1. *Time resolved records*

Typical records of the nozzle supply pressure and test-section Pitot pressure at two test conditions are shown in figure 5. They demonstrate that reasonably steady flow conditions are maintained in the nozzle for the duration of the test period (approximately 7 to 8 ms) at high and low shock-tunnel pressure levels. Corresponding typical records of the static pressure, surface shear (i.e. skin friction) and heat flux on

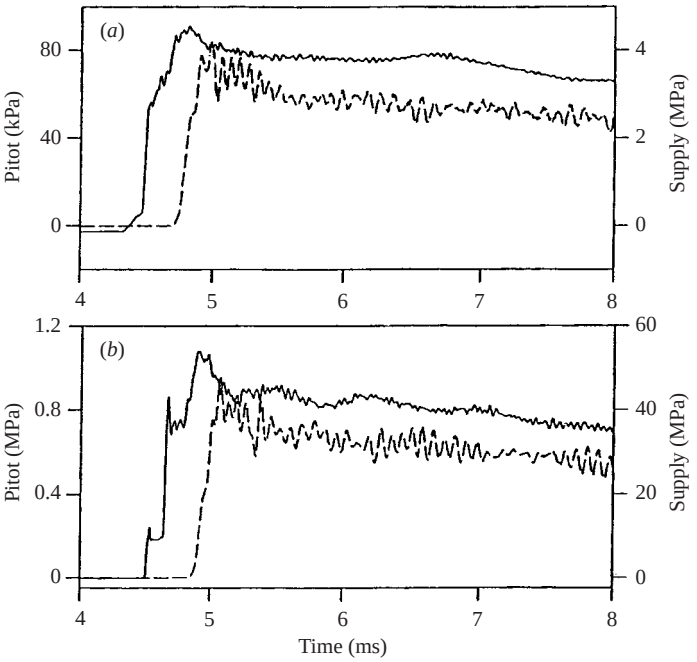

FIGURE 5. Nozzle flow monitoring – typical records (30 μs time averaged) (—, supply; ---, Pitot), (*a*) condition A, (*b*) condition K.

the instrumented surface, together with the ratio between surface shear and heat flux, are shown in figure 6. The records of figure 6(*a*) are for a laminar boundary layer, and those of figure 6(*b*) are for a turbulent boundary layer.

Figures 6(*a*) and 6(*b*) also show a time line marking the major occurrences during the flow event. The nozzle starting process, as outlined by Smith (1966), involves a primary shock, a secondary upstream-facing shock and an unsteady expansion, and these correspond to the times marked as 1, 2 and the interval 3 to 4, respectively. At time 5, a steady ratio of Pitot to nozzle supply pressure indicates that the nozzle had started, while at 6, the ratio of surface shear to heat flux becomes steady. The latter is indicative of steady boundary-layer flow. Times 7 and 8 indicate, respectively, the passage of two and three model lengths of flow of test gas after 5, and 9 points to the arrival of 10% driver gas contamination. The test time begins at 7.

In the laminar boundary-layer case (figure 6*a*), a high level of skin friction is measured in the thin boundary layer developing behind the primary shock. The level then falls following the arrival of the density reduction of the upstream-facing secondary shock, and increases again owing to the density rise associated with passage of the unsteady expansion. It then falls once more as the boundary layer approaches the steady state, to yield the flat-plate skin-friction level predicted by van Driest (1952). In the turbulent case (figure 6*b*), the skin friction during the starting process exhibits the same qualitative behaviour, but the levels recorded are much smaller relative to the steady flow levels than in the laminar case. This is because the nozzle and test section of the shock tunnel were pumped down to similar pressure levels before each test, so that roughly similar density and pressure levels were experienced during the starting process, while the steady flow levels were much higher in the turbulent case. During the indicated test time for the turbulent case, it can be seen

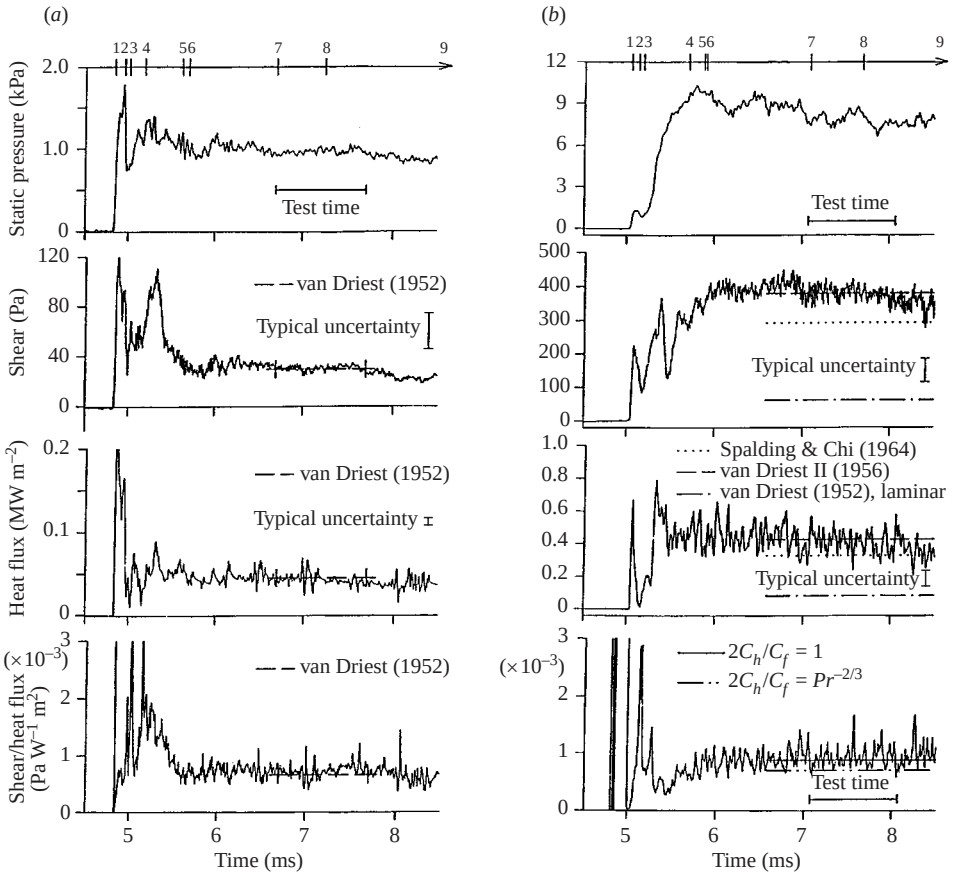

FIGURE 6. Measurements on the instrumented surface – typical records (30 μs time averaged), (*a*) laminar boundary layer, condition A, 370 mm from leading edge, $Re_x = 2.5\times10^5$, (*b*) turbulent boundary layer, condition K, 670 mm from leading edge, $Re_x = 6.7\times10^6$. 1. Primary shock. 2. Secondary shock. 3. Unsteady expansion. 4. Pitot/static steady. 5. Nozzle started, Mach number steady. 6. $\tau/\dot{q}$ steady. 7. Two slugs after nozzle start. 8. Three slugs after nozzle start. 9. 10% contamination.

that the skin-friction level is close to that predicted by van Driest II (1956). As is discussed below, agreement between turbulent skin-friction levels and turbulent theory was a function of flow stagnation enthalpy and unit Reynolds number.

Although the levels of skin friction are seen to be steady and reasonably accurately defined by the records in figure 6, a significant uncertainty is indicated by the error bars, particularly in the laminar case. As noted above, the high level of uncertainty for this condition represents the combination of low shear stress levels and high uncertainty inherent in the pressure calibration technique.

4.2. *Axial distributions*

Axial distributions of Stanton number and skin-friction coefficient measured during the test time are summarized in figures 7, 8 and 9. Stanton number and skin friction were determined using the definitions quoted previously. The three figures correspond to three groupings of the measurements according to the stagnation enthalpy at which they were taken. The nominal value quoted is the average of the stagnation enthalpies noted in table 1 for the test conditions of interest. The test conditions are listed in

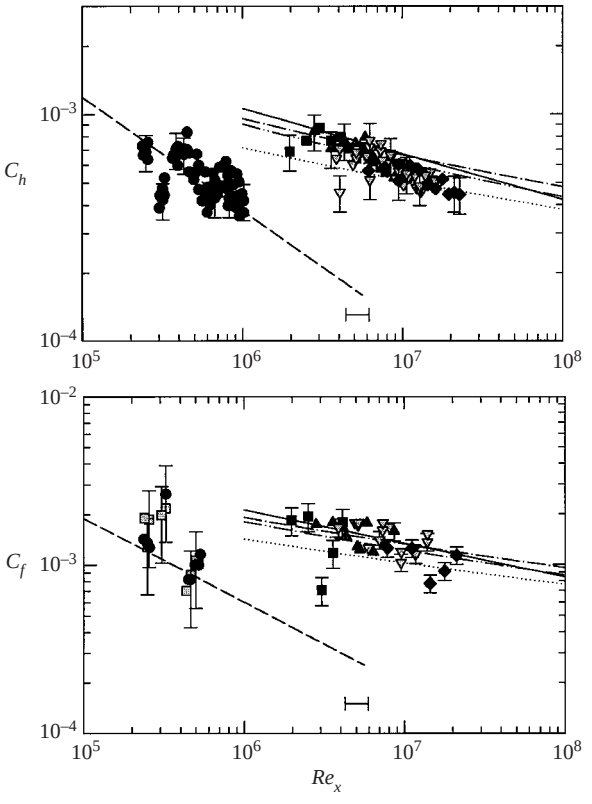

	Symbol	Condition	$Re_u \times 10^6$ (m^{-1})	Direction
van Driest (1952), laminar	●	A	0.67	0º
Spalding & Chi (1964)	▣	A	0.67	180º
van Driest II (1956)	■	D	5.3	0º
Eckert (1955)	▲	H	7.6	0º
Stollery (1976)	▽	K	11	0º
	▲	K	11	180º
	◆	Q	17	0º

FIGURE 7. Measured axial distribution of Stanton number and skin-friction coefficient on instrumented flat plate and comparison with theory, 3.5 MJ kg^{-1} nominal stagnation enthalpy (Reynolds analogy factor of unity assumed for theoretical Stanton number calculations). Representative error bars are shown.

order of increasing unit Reynolds number. Measurements of skin friction were taken with the axis of polarization of the piezoceramic both parallel and anti-parallel to the flow direction, as indicated by the last column of the list of test conditions. It can be seen that the values of skin friction are independent of the polarization direction, thus providing further confirmation of satisfactory operation of the gauges.

Both skin friction and heat transfer display the trend with increasing Reynolds number which is expected as the boundary-layer flow passes from the laminar state, through the transition region, to become turbulent. Based on the heat flux data, transition-onset Reynolds numbers are in the range of 7×10^5–17×10^5. The transition Reynolds numbers indicated by the heat flux are approximately 50% higher than those obtained by He & Morgan (1994) on a flat plate in the same shock tunnel.

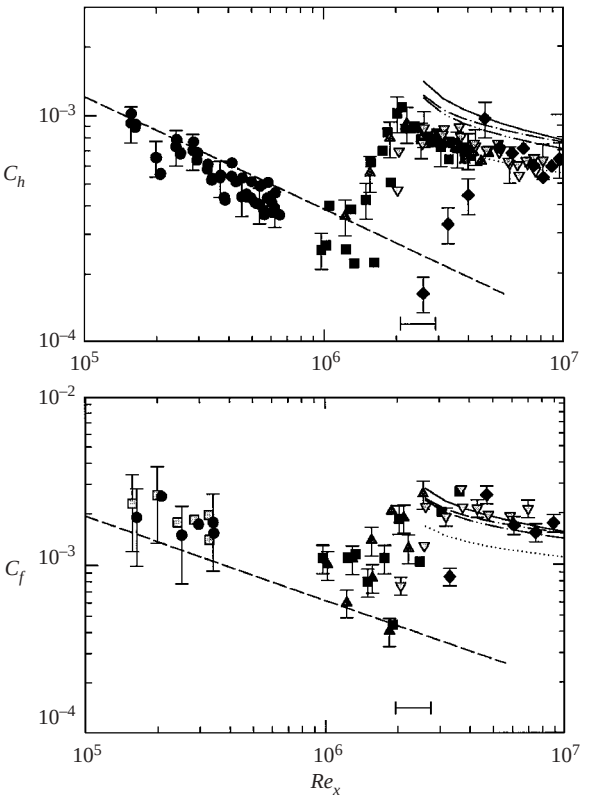

FIGURE 8. Measured axial distribution of Stanton number and skin-friction coefficient on instrumented flat plate and comparison with theory, 6.5 MJ kg^{-1} nominal stagnation enthalpy (Reynolds analogy factor of unity assumed for theoretical Stanton number calculations). Representative error bars are shown.

It is postulated that this is due to the walls of the duct affording shielding from free-stream disturbances to the boundary layer on the instrumented surface, as in Pate & Schueler (1969). For both skin friction and heat transfer, the transition Reynolds numbers increase with unit Reynolds number. This was also found in the ground test investigations of He & Morgan (1994) and Pate & Schueler (1969), for example, and in flight and ballistic-range tests reported by Beckwith (1975) and Potter (1975), respectively. Although strong unit Reynolds-number effects on transition have been observed by many investigators, the effect remains controversial. Hypersonic ground tests (Adam & Hornung 1997) and numerical simulations (Johnson, Seipp & Candler 1997) have indicated that transition can also be dependent on flow stagnation

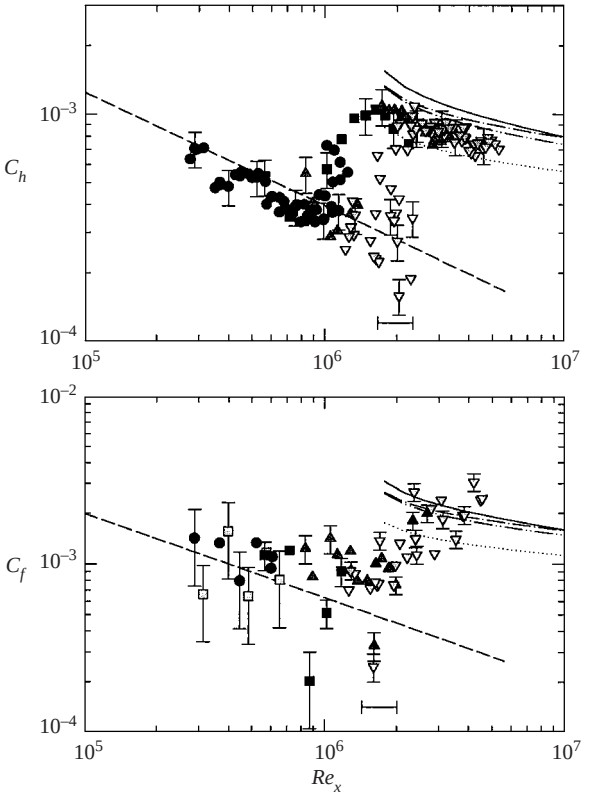

	Symbol	Condition	$Re_u \times 10^6$ (m^{-1})	Direction
van Driest (1952), laminar	●	C	0.79	0°
Spalding & Chi (1964)	□	C	0.79	180°
van Driest II (1956)	■	G	1.5	0°
Eckert (1955)	▲	J	2.3	0°
Stollery (1976)	▽	M	3.5	0°
	▲	M	3.5	180°

FIGURE 9. Measured axial distribution of Stanton number and skin friction coefficient on instrumented flat plate and comparison with theory, 9.0 MJ kg^{-1} nominal stagnation enthalpy (Reynolds analogy factor of unity assumed for theoretical Stanton number calculations). Representative error bars are shown.

enthalpy. Those results showed that increasing stagnation enthalpy had a stabilizing effect on boundary layers.

There is an apparent tendency for the skin friction gauges to indicate transition occurring at higher values of Reynolds number than for the heat flux gauges. This is thought to be due to transition contamination spreading from the streamwise edges of the instrumented surface since, as can be seen in figure 2, the line of heat-flux gauges is closer to the edge than the line of skin-friction gauges. To check this, a number of tests were conducted with a reference heat-flux gauge located on the line of skin-friction gauges, at the same 570 mm station as one of the line of heat-flux gauges. It was found that, below a unit Reynolds number of 3.5×10^6 m^{-1}, the measured heat flux at the reference gauge tended to be lower than that at the adjacent heat-flux gauge and, moreover, the intermittency level tended to be lower. In experiments on

a flat plate at Mach 5.8, Korkegi (1956) found that transition contamination from a sidewall tended to spread at an angle of 5°–6°, and this is consistent with transition in the present experiments spreading from the leading-edge corner of the instrumented surface. At higher values of the unit Reynolds number, the difference between the two heat flux gauges tended to disappear, which is consistent with the region of natural transition moving closer to the leading edge, and the transition region becoming more uniform at the 570 mm station. Thus, the difference between the location of the transition region, as indicated by the skin-friction gauges and the heat-flux gauges in figures 8 and 9, can be ascribed to the effect of sidewall contamination. This implies that the difference should not exist at the higher values of unit Reynolds number and figures 7 and 8 indicate that this is indeed the case.

5. Discussion

In view of existing theory, the laminar and turbulent boundary-layer measurements are now considered in turn. Given the high degree of uncertainty with regard to the accuracy of the turbulent boundary-layer correlations of interest, particular attention is paid to the turbulent measurements.

5.1. *Laminar boundary-layer measurements*

Measured test-time levels of laminar skin friction and heat flux are plotted in figure 10 as a function of the level predicted by van Driest (1952). In spite of the uncertainty associated with the skin-friction measurements in figure 10(*a*), it is evident that, when taken together they indicate a mean level somewhat in excess of the theory. As can be seen in figures 7, 8 and 9, the level of discrepancy between theory and experiment showed no clear trend with stagnation enthalpy or Reynolds number. It can also be seen that the trend of the heat-flux measurements in figure 10(*b*) is slightly below predictions according to van Driest, although, once again, the discrepancy falls within the experimental error.

Using the data of figure 10, the measured Reynolds analogy factor ($2C_h/C_f$) was obtained, yielding a mean value of 0.97 ± 0.43. The error is determined as the root sum square of systematic uncertainty and a 95% confidence interval of the random variations. The Reynolds analogy factor predicted by van Driest (1952) at Mach 6 is 1.26, and the measurements are consistent with that, to within the confidence interval quoted. However, the trend of the results in figure 10 suggests that more accurate measurements may reveal some difference from the theory.

5.2. *Turbulent boundary-layer measurements*

Measurements of compressible turbulent skin friction are traditionally presented on an incompressible plane using the transformation variables first proposed by Spalding & Chi (1964). This allows simultaneous comparison of data with theory for a wide range of test conditions.

The transformed turbulent skin-friction data of the present study are plotted in figure 11. Only data obtained with $Re_x > 1.33\ Re_{x,p}$ are presented, where $Re_{x,p}$ is the Reynolds number at which peak heat transfer occurred. This accords with the criterion for the existence of a turbulent boundary layer used by Cary & Bertram (1974). Although 95% of the measurements were obtained for test flows with 10% or less driver gas contamination, two turbulent measurements with a stagnation enthalpy of 13.1 MJ kg^{-1} and 20% contamination were included in order to augment the data set. The data have been transformed to the incompressible plane using values of F_c and F_{Re_x} as determined using each of the theories of interest. The horizontal axis

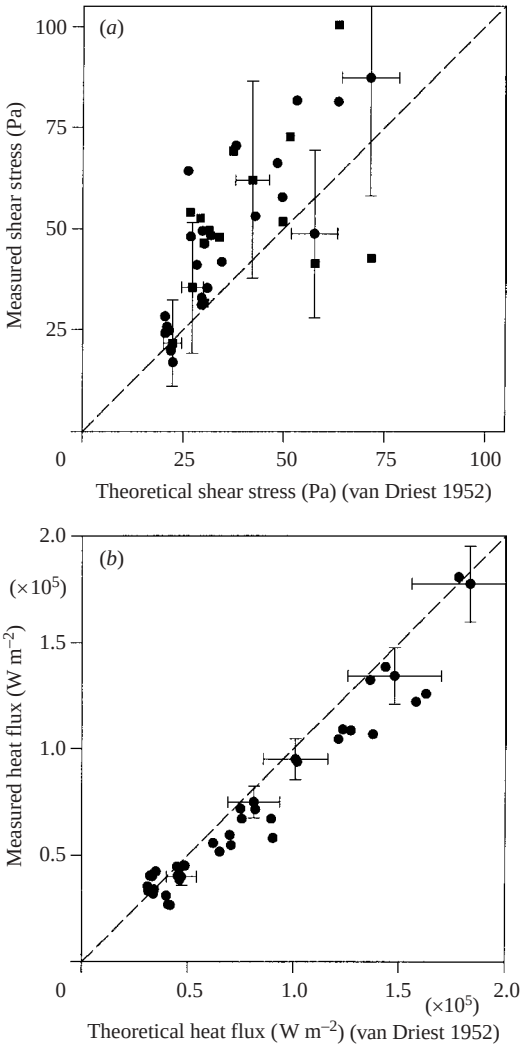

FIGURE 10. Laminar boundary layer measurements, $Re_x = 1.6 \times 10^5 - 6.5 \times 10^5$, $M \approx 6.2$, $h_o = 4.4$–9.1 MJ kg^{-1}, (*a*) skin friction, ●, 0°; ■, 180°; and (*b*) heat flux. Representative error bars are shown.

is based on a Reynolds number that has been adjusted to account for the location of the turbulent virtual origin according to the relation $Re_{x,v} = 0.825\, Re_{x,p}$ (Cary & Bertram 1974). The data are compared with the incompressible Spalding (1962) relation in figures 11(*a*) to 11(*c*). In keeping with the Stollery (1976) method, the data have been transformed and compared with the incompressible one-fifth power law in figure 11(*d*). The transformed experimental results exhibit similar levels of scatter to that observed in the non-adiabatic data reviewed by Cary & Bertram (1974) and Hopkins & Inyoue (1971). The impulse facility data of Holden (1972) and Wallace (1967) also exhibited similar levels of scatter. Although the data transformed using the methods of van Driest II (1956), Eckert (1955) and Stollery (1976) appear to match the overall incompressible C_f level better, the slope of the transformed data does not match the slope of the incompressible relations well.

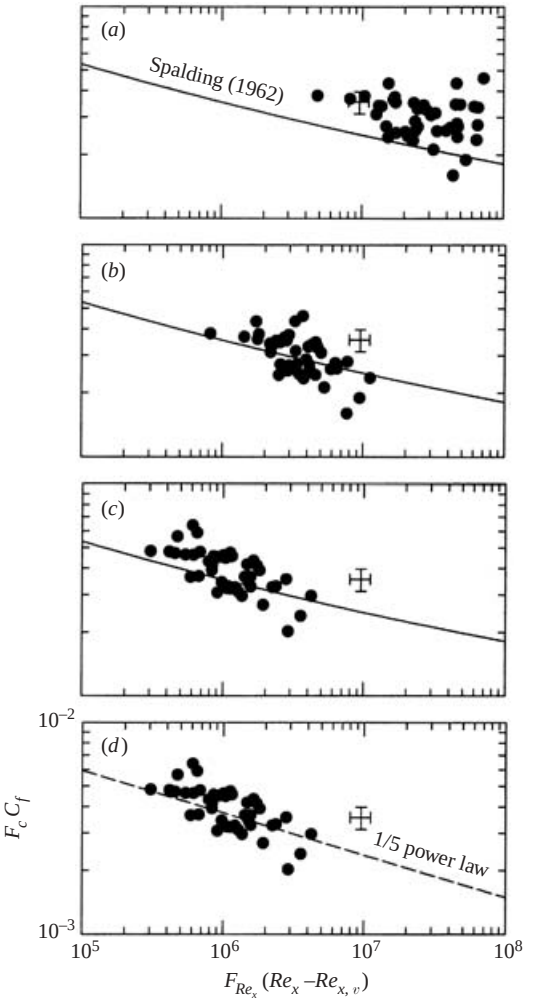

FIGURE 11. Comparison of incompressible theory with transformed skin friction measurements using transformation factors of: (*a*) Spalding & Chi (1964), (*b*) van Driest II (1956), (*c*) Eckert (1955), and (*d*) Stollery (1976).

Because the method of Stollery (1976) is simply an extension of Eckert's reference temperature method, using a less accurate one-fifth power law skin-friction coefficient relation, the technique is not considered further here. However, the level of agreement obtained for the present experiment suggests that the extension to isentropic flows with pressure gradients is feasible for conditions with stagnation enthalpies in the range of 3–13 MJ kg^{-1} and Reynolds numbers in the range of 2.6×10^6–2.1×10^7.

5.2.1. *Additional data*

Before the present measurements are compared further with turbulent theory, it is useful to include the results of additional measurements. These were taken as part of a study of skin friction in a supersonic combustion duct (Goyne *et al.* 1999), and were obtained when no fuel was injected into the duct, and therefore there was no combustion. As described in Goyne *et al.* (1999), the duct was of constant area, with a 48×100 mm^2 rectangular cross-section and a fuel injection strut, 10 mm thick,

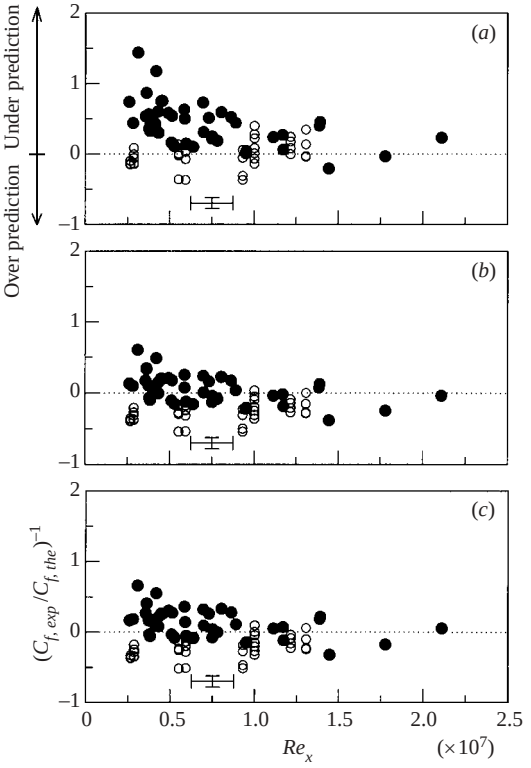

FIGURE 12. Effect of Reynolds number on the accuracy of: (*a*) Spalding & Chi (1964), (*b*) van Driest II (1956), and (*c*) Eckert (1955). ●, test-duct data, $M = 5.3$–6.7. ○, combustion configured duct data, $M = 4.4, 4.5$.

spanning the 100 mm dimension in the midplane of the duct at the duct entrance. The duct was 1320 mm long, and it was instrumented to measure skin friction, heat transfer and pressure in a manner similar to the test duct described above (see figure 2). Measurements were taken at two test conditions; at stagnation enthalpies of $5.7\,\mathrm{MJ\,kg^{-1}}$ and $6.8\,\mathrm{MJ\,kg^{-1}}$, Mach numbers of 4.5 and 4.4, and unit Reynolds numbers of $1.3 \times 10^7\,\mathrm{m^{-1}}$ and $1.2 \times 10^7\,\mathrm{m^{-1}}$, respectively.

As shown by the pressure distributions along the duct (Goyne *et al.* 1999) the central strut in the duct led to pressure variation of $\pm 40\%$ along the duct, involving both positive and negative local pressure gradients, with a maximum magnitude of approximately $250\,\mathrm{kPa\,m^{-1}}$. There was no correlation between the measured skin friction and the direction of these pressure gradients, indicating that the measurements could be taken to correspond to zero pressure gradient flow, and therefore could be used to extend the present data set.

5.2.2. *Effect of Reynolds number*

Consideration is now given to the difference between the present experiments and the theories of Spalding & Chi (1964), van Driest II (1956) and Eckert (1955), respectively. First, the variation of this difference, normalized by the theoretical level, is presented as a function of Reynolds number in figure 12. This serves to confirm the conclusion from figure 11, namely, the results for the test duct display better

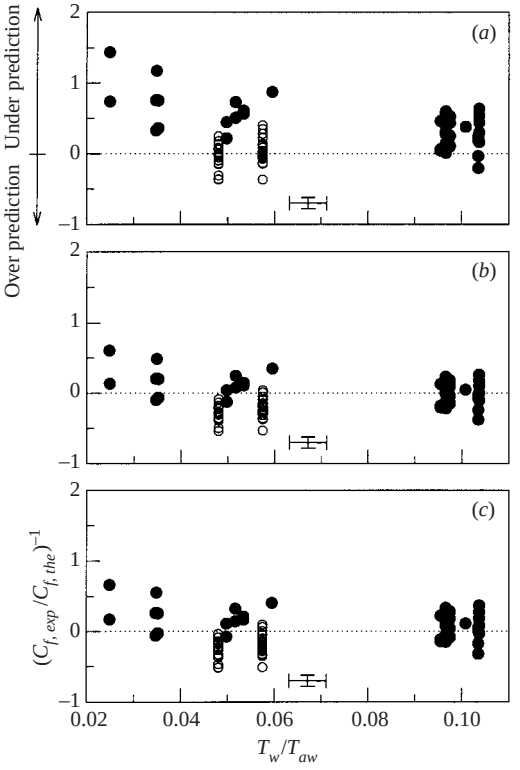

FIGURE 13. Effect of adiabatic wall temperature ratio on the accuracy of: (*a*) Spalding & Chi (1964), (*b*) van Driest II (1956), and (*c*) Eckert (1955), (note: driver contamination >10% for $T_w/T_{aw} < 0.03$). Key as in figure 12.

agreement with van Driest II (1956) and Eckert (1955) than with Spalding & Chi (1964). However, for the combustion configured duct, Spalding & Chi agrees best with the experiments. This apparent disagreement between the test-duct and combustion-duct experiments can be explained by considering the variation of the observed normalized differences between experiment and theory, or 'errors', with the ratio of wall to adiabatic wall temperature and flow unit Reynolds number.

5.2.3. *Effect of* T_w/T_{aw}

The variation of the errors for each theory is plotted as a function of the ratio of wall to adiabatic wall temperature in figure 13. As previously discussed, it is expected that all of the theories will progressively overpredict the skin friction level if the wall temperature ratio trends, observed by other investigators, are extrapolated below $T_w/T_{aw} \approx 0.1$–0.2. It is also expected that van Driest II (1956) will overpredict more than Spalding & Chi (1964) for such conditions. For actual conditions near $T_w/T_{aw} = 0.1$ it can be seen in figure 13 that the test-duct data agree best with van Driest II (1956) and Eckert (1955) and the theory of Spalding & Chi (1964) generally underpredicts. As the wall temperature ratio is reduced, the test-duct data follow a trend contrary to that expected, displaying increasing underprediction by theory as T_w/T_{aw} is reduced. The combustion duct measurements, however, at $T_w/T_{aw} \approx 0.05$, exhibit the expected trend with temperature ratio when the results are compared with the test duct measurements near $T_w/T_{aw} = 0.1$. The average difference between

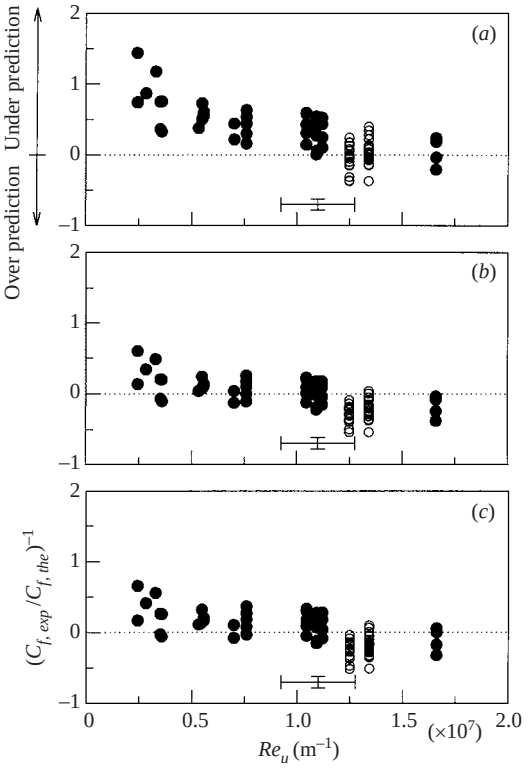

FIGURE 14. Effect of unit Reynolds number on the accuracy of: (*a*) Spalding & Chi (1964), (*b*) van Driest II (1956), and (*c*) Eckert (1955), (note: driver contamination >10% for $Re_u < 2.5 \times 10^6$ m^{-1}). Key as in figure 12.

Spalding & Chi (1964) and van Driest II (1956) with the combustion duct data is of the same order as that observed by Hopkins & Inyoue (1971) and Cary & Bertram (1974) for the high-enthalpy impulse facility measurements of Heronimus (1966), Wallace & McLaughlin (1966), Wallace (1967) and Holden (1972) (with T_w/T_{aw} near 0.14).

5.2.4. *Effect of unit Reynolds number*

The conflict between the wall-temperature trends for the test-duct and combustion-duct experiments can be resolved by plotting the error variation as a function of test-flow unit Reynolds number. The result is shown in figure 14 and it can be seen that all the theories underpredict at low unit Reynolds numbers. For the test-duct experiment, conditions with a low T_w/T_{aw} had a high corresponding stagnation enthalpy and low free-stream density and this resulted in a flow with a corresponding low unit Reynolds number. The high relative levels of $C_{f,exp}$ at low unit Reynolds number in figure 14 therefore correspond to the low-temperature ratio data of figure 13. Because the location of the transition region on the instrumented plates is a function of the unit Reynolds number, it would appear that the location of the transition process may have an influence on the turbulent measurements at low wall temperature ratios and low unit Reynolds numbers.

Hypersonic turbulent boundary-layer experiments are always at risk of downstream effects from the transition region. Such a case may be expected when it is considered

that turbulent spot and transition spreading angles decrease as the free-stream Mach number is increased (e.g. Clark, Jones & LaGraff 1994; Korkegi 1956). Hence, the end of the transition region may not be as uniform or the transition process as complete as for lower-Mach-number flows. In fact, Bradshaw (1977) commented that low-Reynolds-number effects and memories of transition are likely to have affected many hypersonic data sets. Impulse facility data are likely to be no exception. As mentioned in § 2, when Holden (1972) commented on the disagreement between the theory of Spalding & Chi (1964) and high-Mach-number impulse-facility skin-friction data, the question was raised of whether the disagreement was the result of a low-Reynolds-number effect or an inadequacy of the theory. It was concluded that only boundary-layer surveys could provide the complete answer.

Although velocity-profile data of sufficient accuracy is unavailable for impulse-facility flat-plate turbulent-boundary-layer experiments, surveys have been conducted in intermittent facilities at modest stagnation enthalpies (e.g. Hopkins *et al.* 1972; Albertson & Ash 1991). Albertson & Ash (1991), in particular, obtained boundary-layer Pitot profiles near Mach 5.5 with an adiabatic wall temperature ratio near 0.19. This temperature ratio is lower than that obtained in other hypersonic boundary-layer studies. The authors compared the location of the peak measured wall heat flux with the point where the boundary-layer velocity profiles and shape factors matched the equilibrium turbulent-boundary-layer case (as defined by low-speed work). The authors concluded that, for the test conditions ($Re_x = 8\times10^6$–39×10^6), the Reynolds number required for turbulent behaviour to be fully displayed throughout the boundary layer, following transition, was approximately three times the Reynolds number corresponding to the end of transition as indicated by the peak heat flux. The results show that at low T_w/T_{aw} and hypersonic Mach numbers, effects of transition do persist well downstream of a transition region that is defined using wall heat-flux data. This indicates that Cary & Bertram's definition of a turbulent boundary layer of $Re_x > 1.33Re_{x,p}$, which is based on the peak heat flux, is not conservative enough for the tested conditions of the present experiments.

Returning to the unit Reynolds-number variation presented in figure 14, it can be seen that the high unit Reynolds-number data agrees best with the theory of Spalding & Chi (1964). The correlations of van Driest II (1956) and Eckert (1955) generally overpredict at such conditions. If the finding of Albertson & Ash (1991) is applied to the present turbulent data, then most of the points below a unit Reynolds number of $1.2\times10^7\,\mathrm{m}^{-1}$ will be omitted from the graphs because they are too close to the location of peak heat flux. The process of elimination is not straightforward, however, because above a unit Reynolds number of approximately $8\times10^6\,\mathrm{m}^{-1}$, the point of peak heat flux was upstream of the first heat transfer measurement station and hence the point of peak heat flux was not precisely known. However, if a conservative approach is adopted and the peak heat flux is assumed to be at the first heat flux measurement station for the high unit Reynolds-number runs, (instead of $x_p = 0$), then 95% of all the measurements below a unit Reynolds number of $1.2\times10^7\,\mathrm{m}^{-1}$ do not possess Reynolds numbers that are three times larger than the Reynolds number at the peak heat flux. On average, for data with a unit Reynolds number above $1.2\times10^7\,\mathrm{m}^{-1}$, Spalding & Chi (1964) underpredict by (1 ± 11)% and van Driest II (1956) and Eckert (1955) overpredict by (25 ± 8)% and (21 ± 8)%, respectively. Here, the quoted values represent the mean of the errors for each theory and the uncertainties are calculated as the root sum of the squares of the uncertainty representing a 95% confidence interval and the systematic uncertainty of experiment. These results would lead to the conclusion that Spalding & Chi (1964) is the most

appropriate correlation for a high-enthalpy fully developed turbulent boundary layer on a cold wall. This concurs with the low-wall-temperature ratio data findings of Cary & Bertram (1974) and Hopkins & Inyoue (1971), (for $T_w/T_{aw} \approx 0.14$), and with Holden's (1972) low-Mach-number data set ($M < 10, 1 \leqslant h_0 \leqslant 2\,\mathrm{MJ\,kg^{-1}}$). It must be kept in mind, however, that below a unit Reynolds number of approximately $3.5 \times 10^6\,\mathrm{m^{-1}}$, as discussed above, transverse transition contamination is expected to affect the transition zone. The downstream turbulent boundary layer may also be affected for such conditions and hence, the present very low unit Reynolds data may be affected by both transverse transition and natural transition remnants.

The conclusion can be drawn then, that for high Mach number, high stagnation enthalpy flows on cold flat surfaces, the theory of Spalding & Chi (1964) will adequately predict turbulent boundary-layer skin friction, provided the boundary layer has reached an equilibrium state. Such is the case when the flow unit Reynolds number is high and the boundary layer has sufficient distance, downstream of the transition region, to relax from the transitional to the fully turbulent state. This is particularly important with regard to hypersonic flows because transition Reynolds numbers are always high and turbulent spot spreading and merger rate is low.

5.2.5. *Turbulent Reynolds analogy factor*

Before leading to the conclusion, the measured levels of turbulent Reynolds analogy factor are considered. The skin-friction and heat-flux data, originally deemed turbulent using the Cary & Bertram (1974) criteria ($Re_x > 1.33 Re_{x,p}$) are presented in figure 15 in the form of measured Reynolds analogy factor. Both the test-duct and combustion-duct data are included. Figure 15(*a*) depicts the variation of the factor as a function of wall to stagnation enthalpy ratio. The test-duct data show the general trend of decreasing Reynolds analogy factor as h_w/h_0 is decreased. The data for both experiments scatter about unity, a value typically suggested for high-enthalpy hypersonic turbulent boundary layers (Wallace 1967; Cary 1970; Holden 1972; Keener & Polek 1972). In fact, the mean Reynolds analogy factor for the test-duct and combustion-duct data was 0.86 ± 0.19 and 1.1 ± 0.3, respectively, where the uncertainty is calculated as the root sum of squares of the systematic uncertainty and the uncertainty representing a 95% confidence interval for random variation.

Figure 15(*b*) depicts the variation of measured Reynolds analogy factor with the free-stream unit Reynolds number. The analogy factor can be seen to decrease as the unit Reynolds number decreases. However, in the previous section it was proposed that data with unit Reynolds numbers below approximately $1.2 \times 10^7\,\mathrm{m^{-1}}$ were generally affected by transition remnants for the given experimental models, facility and test conditions. Also, as discussed in that section, below a unit Reynolds number of $3.5 \times 10^6\,\mathrm{m^{-1}}$, transverse transition contamination remnants may also have influenced the downstream turbulent boundary layer. The trend of figure 15(*b*), therefore, may only be an indication that the ratio of Stanton number to skin-friction coefficient falls as transition region influences are increased.

As previously discussed, a low unit Reynolds number generally corresponds to a high h_0 or low h_w/h_0 for the tested conditions. Hence, it would follow that the fall in Reynolds analogy factor with h_w/h_0 in the test-duct data is also a transition memory effect. Figure 15(*c*) presents the data of the present study together with that collected by Holden (1972), Keener & Polek (1972) and Cary (1970). The graph confirms Cary's acceptance of the Chi & Spalding (1966) recommended level of 1.16 for near adiabatic wall conditions.

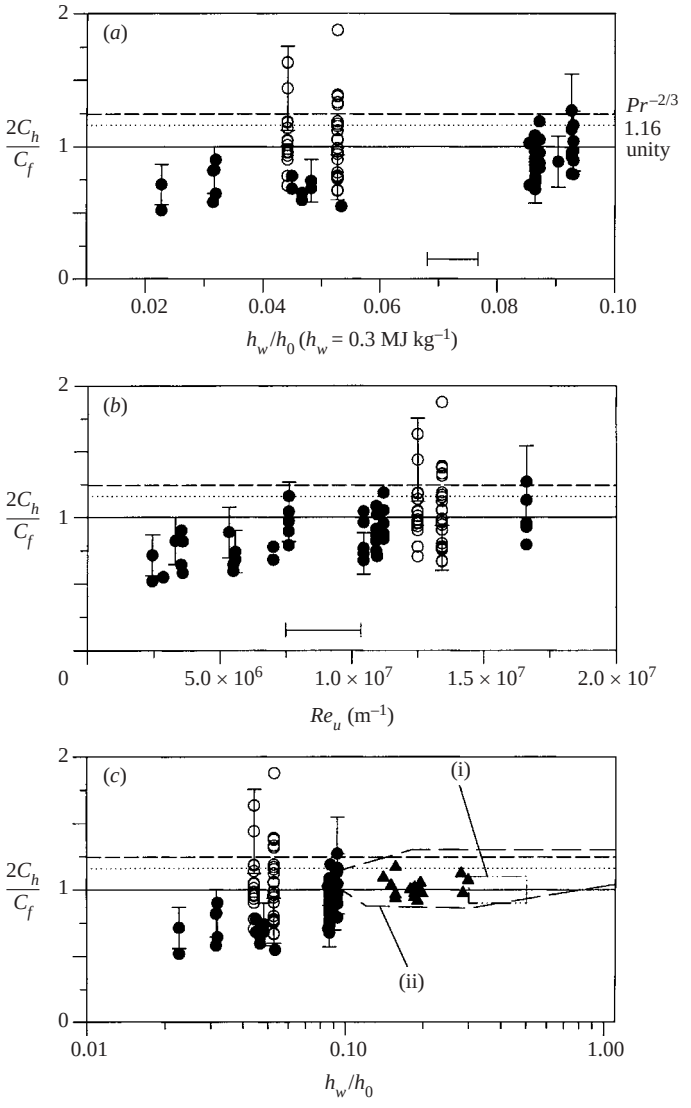

FIGURE 15. Measured Reynolds analogy factor for turbulent boundary layer ($Pr \approx 0.72$, h_0 = shock-tunnel stagnation enthalpy, $Re_x = 2.6 \times 10^6$–2.1×10^7), (*a*) effect of enthalpy ratio (driver contamination >10% for $h_w/h_0 < 0.025$), (*b*) effect of unit Reynolds number (driver contamination >10% for $Re_u < 2.5 \times 10^6\,\mathrm{m}^{-1}$), (*c*) comparison with other flat plate data (Holden 1972 data is plotted as a mean for each test condition). (i) Keener & Polek (1972) M = 6–8; (ii) Cary (1970) M = 2–12; ▲, Holden (1972) (mean data) M = 8–12. Representative error bars are shown. Key as in figure 12.

The lower h_w/h_0 data of Holden (1972) and Keener & Polek (1972) scatter about unity and this is in agreement with the present test-duct data above $h_w/h_0 = 0.08$ and also with the combustion-duct data ($h_w/h_0 \approx 0.05$). Many authors have tentatively proposed that the Reynolds analogy factor falls as h_w/h_0 is decreased (e.g. Wallace 1967; Cary 1970). The present data suggest that for a turbulent high-enthalpy high-Mach-number boundary layer, the Reynolds analogy factor scatters about unity and that any further fall in $2C_h/C_f$ with decreasing h_w/h_0 may only be due to

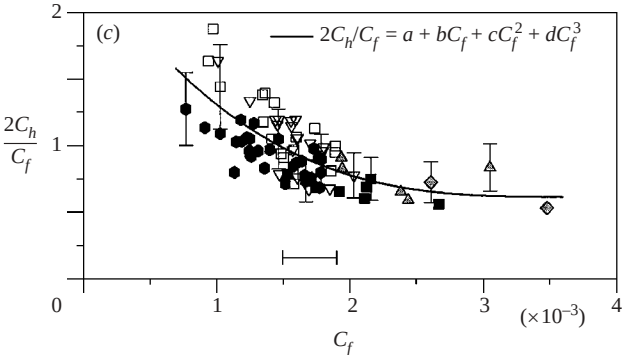

FIGURE 16. Effect of measured skin friction coefficient on Reynolds analogy factor for turbulent boundary layer, Mach number = 4.4–6.7, $Re_u = 2.4 \times 10^6$–$1.7 \times 10^7\ \mathrm{m}^{-1}$, $Re_x = 2.6 \times 10^6$–2.1×10^7. Test duct: ⬢, $3\ \mathrm{MJ\,kg^{-1}}$; ■, 6; ▲, 9; ◆, 13. Combustion configured duct: □, $7\ \mathrm{MJ\,kg^{-1}}$; ▽, 6. (Nominal h_0.) Curve fit: $a = 2.46$, $b = -1.53 \times 10^3$, $c = 4.25 \times 10^5$, $d = -3.95 \times 10^7$. Representative error bars are shown.

low-Reynolds-number effects and transition memory in the boundary layer. This conclusion, however, requires substantiation by further measurements of Reynolds analogy factor for conditions with stagnation enthalpies above approximately $7\ \mathrm{MJ\,kg^{-1}}$ and simultaneously high unit Reynolds numbers.

As a postscript on Reynolds analogy in a high-Mach-number high-enthalpy turbulent boundary layer, figure 16 presents the variation of measured $2C_h/C_f$ with measured C_f. There is a clear trend of decreasing Reynolds analogy factor with increased skin-friction coefficient. Current knowledge of turbulent boundary layers does not explain this effect. The observed trend appears to be independent of unit Reynolds number, stagnation enthalpy and Mach number. This effect has not been observed experimentally in other (lower stagnation enthalpy) investigations and is contrary to the C_f functional dependence of the incompressible von Kármán (1939) relation that was examined by Cary (1970). The results are compared with a fitted cubic correlation curve in figure 16. As the Reynolds analogy factor falls from 1.4, the enthalpy–velocity profile of the boundary layer deviates from the linear form of the Crocco energy relation towards the quadratic form (Wallace 1967). Spina *et al.* (1994) note, however, that for equilibrium turbulent supersonic boundary layers, considerable differences in opinion still exist in relation to the applicability of either the linear or quadratic form. Although lacking a physical interpretation, figure 16 provides a means of obtaining reliable estimates of turbulent wall heat transfer rates when used in conjunction with an appropriate skin-friction prediction method.

6. Conclusions

Simultaneous measurements of skin friction, heat transfer and static pressure have been obtained on a 1500 mm long flat plate that formed one of the inner walls of a rectangular duct. The duct had a cross-section of $120 \times 60\ \mathrm{mm}^2$ at the inlet and the non-instrumented walls each had a 0.5° divergence to allow for boundary-layer displacement. A delta leading edge was used on the surface opposite the instrumented plate and this alleviated leading-edge-interaction wave effects along the duct.

6.1. *Laminar boundary layer*

Laminar measurements of skin friction were obtained for flows with stagnation enthalpies in the range of 4.4–$9.1\ \mathrm{MJ\,kg^{-1}}$ and Reynolds numbers in the range of

1.6×10^5–6.5×10^5. To within experimental uncertainty, the mean test-time levels of skin friction and heat transfer were in agreement with the laminar theory of van Driest (1952). The level of agreement of the skin-friction measurements with theory was independent of Reynolds number, stagnation enthalpy and the 0° and 180° orientation of the gauges to the flow.

6.2. *Transitional boundary layer*

When defined using heat-transfer data, naturally developed transition-onset Reynolds numbers were found to fall in the range of 7×10^5–17×10^5. The transition Reynolds number displayed a dependence on unit Reynolds number. Transverse transition contamination affected the transition region at unit Reynolds numbers below approximately $3.5 \times 10^6\,\mathrm{m}^{-1}$. For these flows, the transition region indicated by the minimum and maximum skin-friction measurements generally corresponded to higher Reynolds numbers than that indicated by the heat-flux measurements. This was consistent with the heat-flux gauges being located closer to sites of transverse transition contamination inception. The results reinforce the need to use the widest possible models for transition studies.

6.3. *Turbulent boundary layer*

Turbulent skin-friction measurements were obtained with Reynolds numbers in the range of 2.6×10^6–21×10^6 for the stagnation enthalpy range of 3–13 $\mathrm{MJ\,kg}^{-1}$. The compressible turbulent boundary-layer correlations of Spalding & Chi (1964), van Driest II (1956), Eckert (1955) and Stollery (1976) were compared with the experimental data. In order to augment the test-duct experimental results, turbulent skin-friction measurements from a duct configured for combustion studies (but without combustion) were included in the analysis. This particular experiment resulted in measurements with Reynolds numbers in the range of 2.6×10^6–13×10^6 and with stagnation enthalpies near $6\,\mathrm{MJ\,kg}^{-1}$.

All of the theories were found to generally underpredict the rise in skin-friction coefficient that occurred at low unit Reynolds number. It was proposed that this was due to the turbulent boundary-layer flow not reaching the turbulent equilibrium state. There was a limited amount of evidence that suggested a trend of increasing overprediction by the theories as the ratio of wall to adiabatic wall temperature fell. Such a trend has also been noted by other investigators but at lower stagnation enthalpy (Hopkins & Inyoue 1971; Bradshaw 1977). The trend, however, was only displayed by the present results, provided the unit Reynolds number of the flow was high.

Over the entire range of the two experiments, the theories of van Driest II (1956) and Eckert (1955) gave the smallest mean difference between theory and experiment. However, the theory of Spalding & Chi (1964) was found to give best agreement at high unit Reynolds number. It was proposed that the heat flux criteria developed by Cary & Bertram (1974) for 'turbulent' data was not conservative enough for the low unit Reynolds-number flows of the present study. This is because the transition region was axially closer to the skin friction measurement stations at low unit Reynolds numbers. As proposed by other investigators for lower stagnation enthalpy flows (Holden 1972; Cary & Bertram 1974), it was inferred that the boundary layer had insufficient length to fully relax from the transitional to the fully turbulent state. The inference was based on the turbulent boundary-layer surveys of Albertson & Ash (1991). These investigators found that an equilibrium turbulent state was only reached far downstream of the location of peak measured heat flux.

Reynolds analogy factor was calculated using the measured levels of skin friction and heat transfer rate. It was found that the factor fell as the wall to stagnation enthalpy ratio was decreased and hence, as the unit Reynolds number fell. Based on the findings of the present study, it was proposed that a reduction of Reynolds analogy factor below unity for a high-Mach-number high-enthalpy boundary layer may only be a low-Reynolds-number and transition-remnant effect. A correlation was found between the Reynolds analogy factor and the measured skin friction coefficient which, though unexplained, offers the possibility of defining the relation between skin friction and heat transfer more accurately for hypersonic turbulent boundary layers.

It is concluded that for turbulent boundary layers approaching the turbulent equilibrium state, the Spalding & Chi (1964) method should be used to predict skin friction coefficient in high-enthalpy high-Mach-number flows ($0.04 \leqslant h_w/h_0 \leqslant 0.09$ or $0.05 \leqslant T_w/T_{aw} \leqslant 0.1$ and $4.4 \leqslant M \leqslant 6.7$). If the heat transfer rate to the wall is to be predicted, then the Spalding & Chi (1964) method should be used in conjunction with a Reynolds analogy factor near unity. If more accurate results are required, then the experimentally observed relationship between Reynolds analogy factor and skin friction coefficient should be applied.

The findings of this study are encouraging for the future engineering of sustained hypersonic flight of slender vehicles. The results indicate that the total component of viscous drag, contributed by fully developed turbulent boundary layers, will match Spalding & Chi (1964) levels. Such levels are generally 20%–30% lower than those predicted by other popular correlations such as van Driest II (1956). According to Reynolds analogy, this will result in heat flux loads that are also 20%–30% lower, and hence, thermal protection system savings will also be possible.

The authors thank J. Brennan and B. Allsop for the part they played in development of the skin-friction gauges. The authors also note their appreciation of the support provided by the Australian Research Council for operation of the shock tunnel T4, and of that provided in the early stages of the project by NASA Langley, through NASA grant NAGW-674.

REFERENCES

Adam, P. H. & Hornung, H. G. 1997 Enthalpy effects on hypervelocity boundary-layer transition: ground test and flight data. *J. Spacecraft Rockets* **34**, 614–619.

Albertson, C. W. & Ash, R. L. 1991 Compressible equilibrium turbulent boundary layers at nonadiabatic wall conditions. *AIAA J.* **29**, 1573–1580.

Anderson, G., Kumar, A. & Erdos, J. 1990 Progress in hypersonic combustion technology with computation and experiment. *AIAA Second Intl Aerospace Planes Conf. Orlando, 29–31 October*, *AIAA*-90-5254.

Beckwith, I. E. 1975 Development of a high Reynolds number quiet tunnel for transition research. *AIAA J.* **13**, 300–306.

Boyce, R. R., Takahashi, M. & Stalker, R. J. 1996 Mass spectrometer measurements of the freestream flow in the T4 free piston shock tunnel. *5th Intl Workshop on Shock Tube Technology, Göttingen.*

Bradshaw, P. 1977 Compressible turbulent shear layers. *Annu. Rev. Fluid Mech.* **9**, 33–54.

Cary, A. M. 1970 Summary of available information on Reynolds analogy for zero-pressure-gradient, compressible, turbulent-boundary-layer flow. *NASA Tech. Note* D-5560.

Cary, A. M. & Bertram, M. H. 1974 Engineering prediction of turbulent skin friction and heat transfer in high-speed flow. *NASA Tech. Note* D-7507.

Chi, S. W. & Spalding, D. B. 1966 Influence of temperature ratio on heat transfer to a flat plate through a turbulent boundary layer in air. *Proc. Third Intl Heat Transfer Conf., Chicago, August*.

Clark, J. P., Jones, T. V. & LaGraff, J. E. 1994 On the propagation of naturally-occurring turbulent spots. *J. Engng Maths* **28**, 1–19.

Coleman, G. T., Osborne, C. & Stollery, J. L. 1973 Heat transfer from a hypersonic turbulent boundary layer on a flat plate. *J. Fluid Mech.* **60**, 257–271.

Davis, D. O., Gessner, F. B. & Kerlick, G. D. 1986 Experimental and numerical investigation of supersonic turbulent flow through a square duct. *AIAA J.* **24**, 1508–1515.

Davis, D. O., Gessner, F. B. & Kerlick, G. D. 1987 Supersonic laminar flow development in a square duct. *AIAA J.* **25**, 175–177.

van Driest, E. R. 1951 Turbulent boundary layer in compressible fluids. *J. Aeronaut. Sci.* **18**, 145–160.

van Driest, E. R. 1952 Investigation of laminar boundary layer in compressible fluids using the Crocco method. *NACA Tech. Note* 2597.

van Driest, E. R. 1956 The problem of aerodynamic heating. *Aeronaut. Engng Rev.* **15**, 26–41.

East, R. A., Stalker, R. J. & Baird, J. P. 1980 Measurements of heat transfer to a flat plate in a dissociated high-enthalpy laminar air flow. *J. Fluid Mech.* **97**, 673–699.

Eckert, E. R. G. 1955 Engineering relations for friction and heat transfer to surfaces in high velocity flow. *J. Aeronaut. Sci.* **22**, 585–587.

Goyne, C. P., Stalker, R. J. & Paull, A. 1999 Shock tunnel skin friction measurement in a supersonic combustor. *J. Propulsion Power* **15**, 699–705.

Goyne, C. P., Stalker, R. J. & Paull, A. 2002 Transducer for direct measurement of skin friction in hypervelocity impulse facilities. *AIAA J.* **40**, 42–49.

Hazelton, D. M. & Bowersox, R. D. W. 1998 Skin friction correlations for high enthalpy flows. *Proc. AIAA 8th Intl Space planes and Hypersonic Systems and Technologies Conf. Norfolk, April, AIAA*-98-1636.

He, Y. & Morgan, R. G. 1994 Transition of compressible high enthalpy boundary layer flow over a flat plate. *Aeronaut. J.* **98**, 25–33.

Heronimus, G. A. 1966 Hypersonic shock tunnel experiments on the W7 flat plate model – expansion side, turbulent flow and leading edge transpiration data. *CAL Rep.* AA-1952-Y-2, February. Cornell Aero. Lab.

Holden, M. S. 1972 An experimental investigation of turbulent boundary layers at high Mach numbers and Reynolds numbers. *NASA* CR-112147.

Hopkins, E. J. & Inouye, M. 1971 An evaluation of theories for predicting turbulent skin friction and heat transfer on flat plates at supersonic and hypersonic Mach numbers. *AIAA J.* **9**, 993–1003.

Hopkins, E. J., Keener, E. R., Polek, T. E. & Dwyer, H. A. 1972 Hypersonic turbulent skin-friction and boundary-layer profiles on nonadiabatic plat plates. *AIAA J.* **10**, 40–48.

Hopkins, E. J., Rubesin, M. W., Inouye, M., Keener, E. R., Mateer, G. C. & Polek, T. E. 1969 Summary and correlation of skin-friction and heat transfer data for a hypersonic turbulent boundary layer on simple shapes. *NASA Tech. Note* D-5089.

Johnson, H. B., Seipp, T. G. & Candler, G. V. 1997 Numerical study of hypersonic reacting boundary layer transition on cones. *AIAA* 97-2567.

von Kármán, T. 1939 The analogy between fluid friction and heat transfer. *Trans. ASME* **61**, 705–710.

Keener, E. R. & Polek, T. E. 1972 Measurements of Reynolds analogy for a hypersonic turbulent boundary layer on a nonadiabatic flat plate. *AIAA J.* **10**, 845–846.

Korkegi, R. H. 1956 Transition studies and skin friction measurements on an insulated flat plate at a Mach number of 5.8. *J. Aeronaut. Sci.* **23**, 97–107.

Lordi, J. A., Mates, R. E. & Moselle, R. J. 1966 Computer program for the numerical simulation of nonequilibrium expansion of reacting gas mixtures. *NASA* CR-472.

Mee, D. J. 1993 Uncertainty analysis of conditions in the test section of the T4 shock tunnel. *Res. Rep.* 4/93, Dept. Mech. Engng, University of Queensland.

Mee, D. J. & Goyne, C. P. 1996 Turbulent spots in boundary layers in a free-piston shock-tunnel flow. *Shock Waves* **6**, 337–343.

Neal, L., Jr 1966 A study of the pressure, heat transfer and skin friction on sharp and blunt flat plates at Mach 6.8. *NASA Tech. Note* D-3312.

Pate, S. R. & Schueler, C. J. 1969 Radiated aerodynamic noise effects on boundary-layer transition in supersonic and hypersonic wind tunnels. *AIAA J.* **7**, 450–457.

Paull, A. 1996 A simple shock tunnel driver gas detector. *Shock Waves* **6**, 309–312.

Paull, A., Stalker, R. J. & Mee, D. J. 1995 Experiments on supersonic combustion ramjet propulsion in a shock tunnel. *J. Fluid Mech.* **296**, 159–183.

Potter, J. L. 1975 Boundary-layer transition on supersonic cones in an aeroballistic range. *AIAA J.* **13**, 270–277.

Schlichting, H. 1979 *Boundary-layer Theory*, 7th edn. McGraw-Hill.

Skinner, K. A. 1994 Mass spectrometry in shock tunnel experiments of hypersonic combustion. PhD thesis, Dept. Mech. Engng, University of Queensland.

Skinner, K. A. & Stalker, R. J. 1996 Mass spectrometer measurements of test gas composition in a shock tunnel. *AIAA J.* **34**, 203–205.

Smith, C. E. 1966 The starting process in a hypersonic nozzle. *J. Fluid Mech.* **24**, 625–640.

Sommer, S. C. & Short, B. J. 1955 Free-flight measurements of turbulent-boundary-layer skin friction in the presence of severe aerodynamic heating at Mach numbers from 2.8 to 7.0. *NACA Tech. Note* 3391.

Spalding, D. B. 1962 A new analytical expression for the drag of a flat plate valid for both the turbulent and laminar regimes. *Intl J. Heat Mass Transfer* **5**, 1133–1138.

Spalding, D. B. & Chi, S. W. 1964 The drag of a compressible turbulent boundary layer on a smooth flat plate with and without heat transfer. *J. Fluid Mech.* **18**, 117–143.

Spina, E. F., Smits, A. J. & Robinson, S. K. 1994 The physics of supersonic turbulent boundary layers. *Annu. Rev. Fluid Mech.* **26**, 287–319.

Stainback, P. C. & Weinstein, L. M. 1967 Aerodynamic heating in the vicinity of corners at hypersonic speeds. *NASA Tech. Note* D-4130.

Stollery, J. L. 1976 Supersonic turbulent boundary layers: some comparisons between experiment and a simple theory. *Aeronaut. Q.* **27**, 87–98.

Wallace, J. E. 1967 Hypersonic turbulent boundary-layer studies at cold wall conditions. *Heat Transfer and Fluid Mech. Inst., California, February*, pp. 427–451; also *NASA* CR-82425.

Wallace, J. E. & McLaughlin, E. J. 1966 Experimental investigations of hypersonic, turbulent flow and laminar leeward-side flow on flat plates. *TR AFFDL*-TR-66-63, vol. 1, Cornell Aeronautical Laboratory.

White, F. M. 1991 *Viscous Fluid Flow*, 2nd edn. McGraw-Hill.

Young, F. L. 1965 Experimental investigation of the effects of surface roughness on compressible turbulent boundary layer skin friction and heat transfer. *Rep. DRL*-532, CR-21, Defence Res. Lab. University of Texas.